Article

Quinone-mediated hydrogen anode for non-aqueous reductive electrosynthesis

https://doi.org/10.1038/s41586-023-06534-2

Received: 13 April 2023

Accepted: 11 August 2023

Published online: 21 August 2023

Check for updates

Jack Twilton[1,4], Mathew R. Johnson[1,4], Vinayak Sidana[1], Mareena C. Franke[1], Cecilia Bottecchia[2], Dan Lehnherr[2], François Lévesque[2], Spring M. M. Knapp[1], Luning Wang[1], James B. Gerken[1], Cynthia M. Hong[2], Thomas P. Vickery[2], Mark D. Weisel[2], Neil A. Strotman[2], Daniel J. Weix[1]✉, Thatcher W. Root[3]✉ & Shannon S. Stahl[1]✉

Electrochemical synthesis can provide more sustainable routes to industrial chemicals[1–3]. Electrosynthetic oxidations may often be performed 'reagent-free', generating hydrogen (H_2) derived from the substrate as the sole by-product at the counter electrode. Electrosynthetic reductions, however, require an external source of electrons. Sacrificial metal anodes are commonly used for small-scale applications[4], but more sustainable options are needed at larger scale. Anodic water oxidation is an especially appealing option[1,5,6], but many reductions require anhydrous, air-free reaction conditions. In such cases, H_2 represents an ideal alternative, motivating the growing interest in the electrochemical hydrogen oxidation reaction (HOR) under non-aqueous conditions[7–12]. Here we report a mediated H_2 anode that achieves indirect electrochemical oxidation of H_2 by pairing thermal catalytic hydrogenation of an anthraquinone mediator with electrochemical oxidation of the anthrahydroquinone. This quinone-mediated H_2 anode is used to support nickel-catalysed cross-electrophile coupling (XEC), a reaction class gaining widespread adoption in the pharmaceutical industry[13–15]. Initial validation of this method in small-scale batch reactions is followed by adaptation to a recirculating flow reactor that enables hectogram-scale synthesis of a pharmaceutical intermediate. The mediated H_2 anode technology disclosed here offers a general strategy to support H_2-driven electrosynthetic reductions.

Electrochemical HOR is well established in fuel cells (Fig. 1a). Humidified H_2 gas is delivered to the anode within a membrane–electrode assembly (MEA) that incorporates gas-diffusion, catalyst and proton-exchange-membrane layers. This approach is not readily adapted to organic electrosynthesis in non-aqueous media because protons derived from HOR migrate to the cathode through the proton-exchange-membrane layer accompanied by substantial amounts of water. For typical electrosynthetic reductions, water would accumulate in concentrations of 1–5 M in the cathode compartment[16], markedly changing the reaction medium and complicating moisture-sensitive reduction reactions. Gas-diffusion electrodes (GDEs) offer an alternative approach to achieve non-aqueous electrochemical HOR and they have been used recently to support lithium-mediated N_2 reduction[9,11]. Contemporary efforts are directed towards mechanistic studies and catalyst-design efforts to address the kinetic limitations of electrocatalytic HOR in organic solvent[7,8,11].

This study was initiated to explore another strategy, whereby thermal catalytic hydrogenation of a redox-active molecule is used to support indirect electrochemical HOR. Quinone hydrogenation is well established in organic solvent and is featured in the industrial anthraquinone process for hydrogen peroxide synthesis[17]. Separately, good electrochemical properties of quinones are evident from their recent use in organic redox-flow batteries[18,19] and mediated fuel cells[20]. The reversible chemical/electrochemical interconversion of quinone and hydroquinone (Fig. 1b) provides the basis for a quinone-mediated H_2 anode to support electrosynthetic reduction reactions. Ni-catalysed XEC reactions were selected as the cathode reaction for this study (Fig. 1c,d). The widespread use of stoichiometric metal reductants (Zn, Mn) in these reactions complicates large-scale applications, owing to the non-uniform reactivity and particle properties of these metals, difficulty in suspending dense metal powders in batch reactors and formation of stoichiometric Zn or Mn salts as waste[21]. These issues have motivated considerable efforts to develop electrochemical variants of these reactions[22–31] and H_2 offers the most atom-economical and sustainable source of electrons for these reactions. Although H_2 introduces potential safety hazards, it is often the preferred reagent for chemical reductions in industrial manufacturing[32].

Ni-catalysed coupling of aryl and alkyl halides to form $C(sp^2)$–$C(sp^3)$ bonds is among the most thoroughly developed class of XEC reactions[33] (see Fig. 1c). For this study, we selected a Ni catalyst composed of $NiBr_2$ and a dual dtbbpy/ttbtpy ligand system, adapted from recent reports[26,29] (dtbbpy = 4,4′-di-*tert*-butyl-2,2′-bipyridine, ttbtpy = 4,4′,4″-tri-*tert*-butyl-2,2′:6′,2″-terpyridine). Selection of components for the mediated H_2 anode was inspired by recent reports

[1]Department of Chemistry, University of Wisconsin–Madison, Madison, WI, USA. [2]Process Research & Development, Merck & Co., Inc., Rahway, NJ, USA. [3]Department of Chemical and Biological Engineering, University of Wisconsin–Madison, Madison, WI, USA. [4]These authors contributed equally: Jack Twilton, Mathew R. Johnson. ✉e-mail: dweix@wisc.edu; twroot@wisc.edu; stahl@chem.wisc.edu

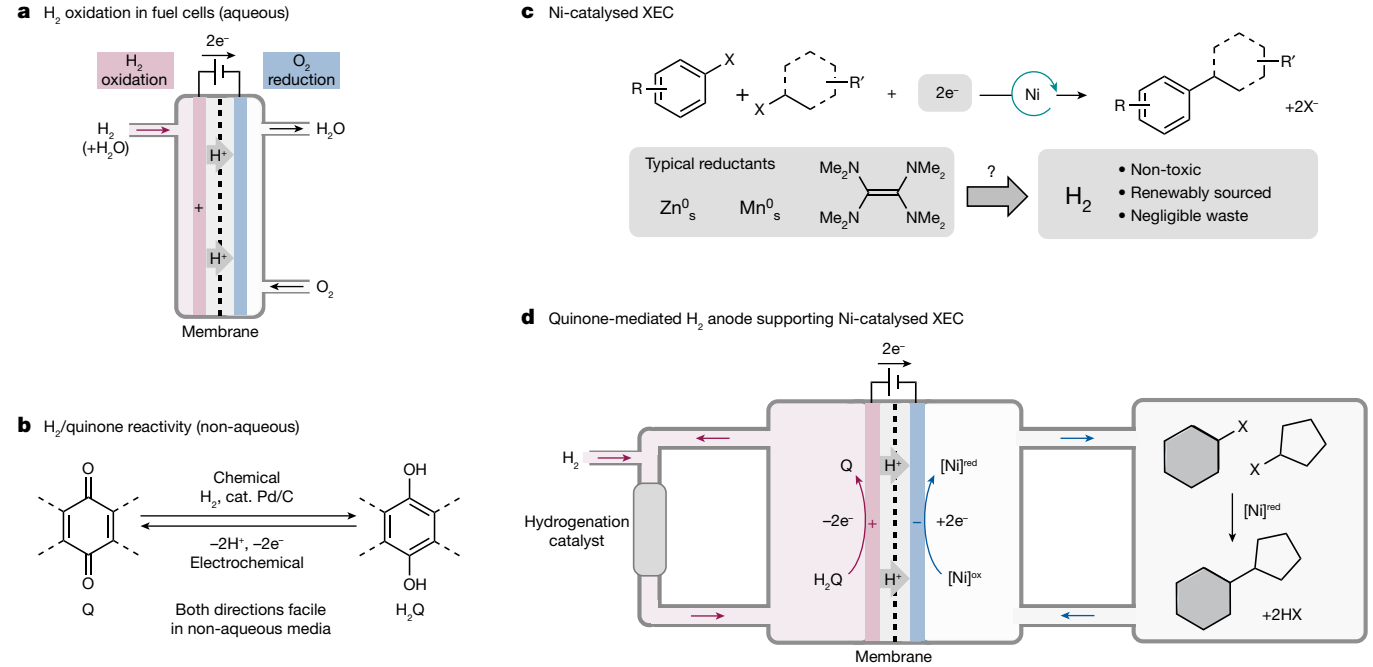

Fig. 1 | Strategy to allow the use of H_2 as a source of electrons for Ni-catalysed XEC in organic solvent. a, The electrochemical HOR is a key feature of fuel cells. The essential role of water in supporting HOR and transport of water through the membrane limits use of this method in non-aqueous electrochemistry. **b**, Catalytic hydrogenation quinones and electrochemical oxidation of hydroquinones are facile in organic solvents. **c**, Ni-catalysed XEC is an important and growing class of reduction reactions that would benefit from the ability to use H_2 as a reductant. **d**, Quinone-mediated H_2 anode concept, designed to support electrochemical Ni-catalysed XEC.

using anthraquinones and other substituted quinones under aqueous conditions for redox-flow batteries[18,19] and mediated fuel cells[34,35]. Sodium anthraquinone-2-sulfonate (AQS) exhibits good solubility in polar organic solvents, such as *N*,*N*-dimethylformamide (DMF) and *N*-methyl-2-pyrrolidone (NMP). Cyclic voltammetry (CV) analysis of AQS in NMP revealed a redox potential of −0.59 V versus a ferrocenium/ferrocene (Fc^+/Fc) reference potential (Fig. 2a and Extended Data Fig. 1c). This value is 200 mV higher than the H^+/H_2 potential (−0.79 V), measured under the same conditions using CV and open-circuit-potential (OCP) methods (Fig. 2a and Extended Data Fig. 1a). CV analysis was also used to investigate the redox potentials of nickel bromide complexes bearing the dtbbpy and ttbtpy ligands. The measured two-electron and one-electron reduction potentials of these complexes range from −1.3 to −2.1 V versus Fc^+/Fc (Fig. 2a and Extended Data Fig. 1b). The 0.5–1.3 V difference between the redox potentials of H_2 and catalytically relevant Ni complexes confirms that H_2 lacks the driving force necessary to serve as a chemical reductant for thermal Ni-catalysed XEC. Application of an external voltage, however, allows the potential of electrons from H_2 to be adjusted to the potential needed to support the reactions under electrochemical conditions.

The relative redox potentials of H_2 and AQS indicate that AQS hydrogenation is thermodynamically favourable and experimental tests further show that this reaction is kinetically facile when using a heterogeneous Pd/C catalyst with 1 atm of H_2 at room temperature (Extended Data Fig. 2). These results provided a starting point for H-cell batch electrolysis experiments to test a mediated H_2 anode system in combination with cathodic Ni-catalysed XEC (Fig. 2b). Both half-cells feature indirect electrochemical processes with a combination of electrochemical and off-electrode chemical reactions (Fig. 2b, grey and coloured boxes, respectively). Optimization of the H_2-coupled Ni-catalysed XEC reaction conditions used ethyl 4-bromobenzoate and (3-bromopropyl) benzene as the aryl and alkyl electrophiles (Fig. 2c). Individual reaction parameters were varied (Extended Data Fig. 3 and the Supplementary Information) to identify the most effective conditions for this substrate. The following conditions led to formation of the desired $C(sp^2)$–$C(sp^3)$ XEC product in 82% yield: 0.2 M aryl bromide as the limiting reagent, 1.25 equiv of the alkyl bromide, a 10 mol% catalyst composed of $NiBr_2 \cdot 3H_2O$ with a 4:1 ratio of dtbbpy/ttbtpy ligands and 0.2 M LiBr as the supporting electrolyte in NMP. The anode chamber contained 5 wt% Pd/C (with a Pd loading of 5 mol% relative to the Ar–Br), 20 mol% AQS, 2 equiv Na_2CO_3 and 0.2 M LiBr in NMP. These or closely related conditions proved to be effective with a broad range of pharmaceutically relevant coupling partners (Fig. 2d). For example, both electron-rich and electron-poor aryl bromides undergo coupling in high yields (**1**–**4** and **9**) and the method proceeds well with a pendant arylboronic ester group (**5**), a standard reactive group in cross-coupling reactions. This Ni/dtbbpy/ttbtpy catalyst system tolerates a range of Lewis basic nitrogen heterocycles, which are prevalent in drug candidates. Examples include pyridines substituted at the 2-position, 3-position and 4-position (**10**, **11**, **13**–**18**), pyrimidine (**12**), indole (**19**) and indazole (**20**, **21**). This catalyst system is also effective with different primary and secondary alkyl bromides (**14**–**18**, **21**), including those with strained rings (**15**, **21**) and *tert*-butoxycarbonyl (Boc)-protected primary and secondary amines (**1**–**13**, **19**, **20**). These results show excellent compatibility between the mediated H_2 anode and Ni-catalysed XEC reactions and they often exceed those obtained in previous studies using the same catalyst system with a tertiary amine reductant[26,29].

The primary merits of the mediated H_2 anode will be experienced at larger scale. Therefore, subsequent efforts focused on development of a flow cell that could be integrated with a parallel-plate electrochemical reactor. To facilitate development and testing of the system, the mediated anode was paired with a simple cathodic electron-transfer reaction, involving reduction of Bobbitt's salt, [$ACT^+BF_4^-$], an oxoammonium compound derived from 4-acetamido-2,2,6,6-tetramethylpiperidine-*N*-oxyl (ACT; Fig. 3a). This reaction was selected for anode-characterization studies because one-electron reduction of ACT^+ to the aminoxyl ACT exhibits good electrochemical kinetics and thus will not limit anodic performance. The mediated

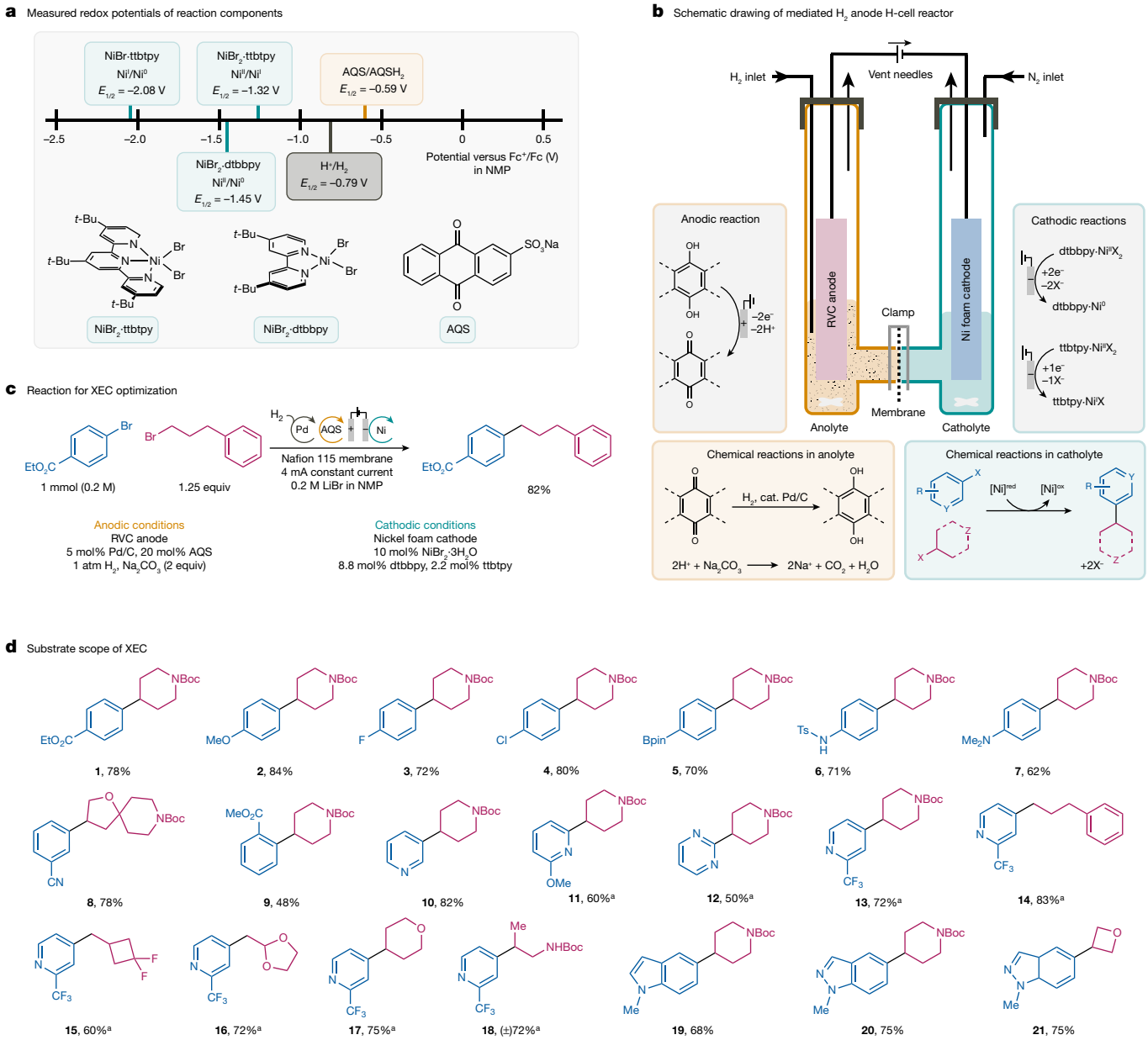

Fig. 2 | Voltammetric analysis and electrochemical Ni XEC using a mediated H_2 anode in an H-cell. a, Redox potentials measured for H_2, the anthraquinone mediator and Ni catalyst species show that the potential of H_2 is insufficient to drive Ni XEC in the absence of an electrochemical bias. **b**, H-cell schematic illustrating the electrochemical and chemical processes in the anolyte and catholyte compartments. **c**, XEC substrates used for reaction testing and optimized reaction conditions. **d**, Ni XEC products obtained using the H-cell with a mediated H_2 anode, shown in **b**, under conditions identical or similar to those in **c** (see the Supplementary Information for details). [a]Heteroaryl chloride used instead of the bromide.

anode was designed with two separate flow loops sharing a common liquid reservoir. The hydrogenation loop includes a packed-bed reactor containing Pd/C and is used to support continuous hydrogenation of AQS to $AQSH_2$. The electrolysis loop circulates the mediator/electrolyte solution over the anode, resulting in electrochemical oxidation of $AQSH_2$ to AQS. This mediated-anode design provides a unique opportunity to manage protons generated during electrochemical oxidation of $AQSH_2$. The protons are retained in flowing solution, rather than passing through the membrane, and they are transported back into the anolyte reservoir, in which they undergo neutralization by Li_2CO_3. This neutralization exchanges H^+ with Li^+ ions in solution and results in the transport of lithium ions rather than protons through the Nafion membrane during electrolysis. Inductively coupled plasma optical emission spectroscopy analysis of the catholyte solution during operation of the mediated H_2 anode showed a linear increase in $[Li^+]$, with a magnitude that directly correlates with the charge passed during electrolysis (Extended Data Fig. 5c). This feature is in contrast to conventional H_2 anode configurations, which are designed to ensure efficient proton transport through the membrane to support O_2 reduction or other cathodic reactions. In this system, proton migration would have a deleterious effect, resulting in parasitic H_2 evolution at the cathode and/or generating undesirable by-products through protonolysis of organometallic Ni intermediates (Extended Data Fig. 6). Thus, the mediated H_2 anode enables the use of H_2 as a source of electrons—without protons—for the cathodic reduction reaction.

To monitor the interplay between the hydrogenation and electrolysis loops, in situ ultraviolet–visible spectroscopy was used to follow redox speciation of the quinone mediator in the anolyte reservoir. Operation

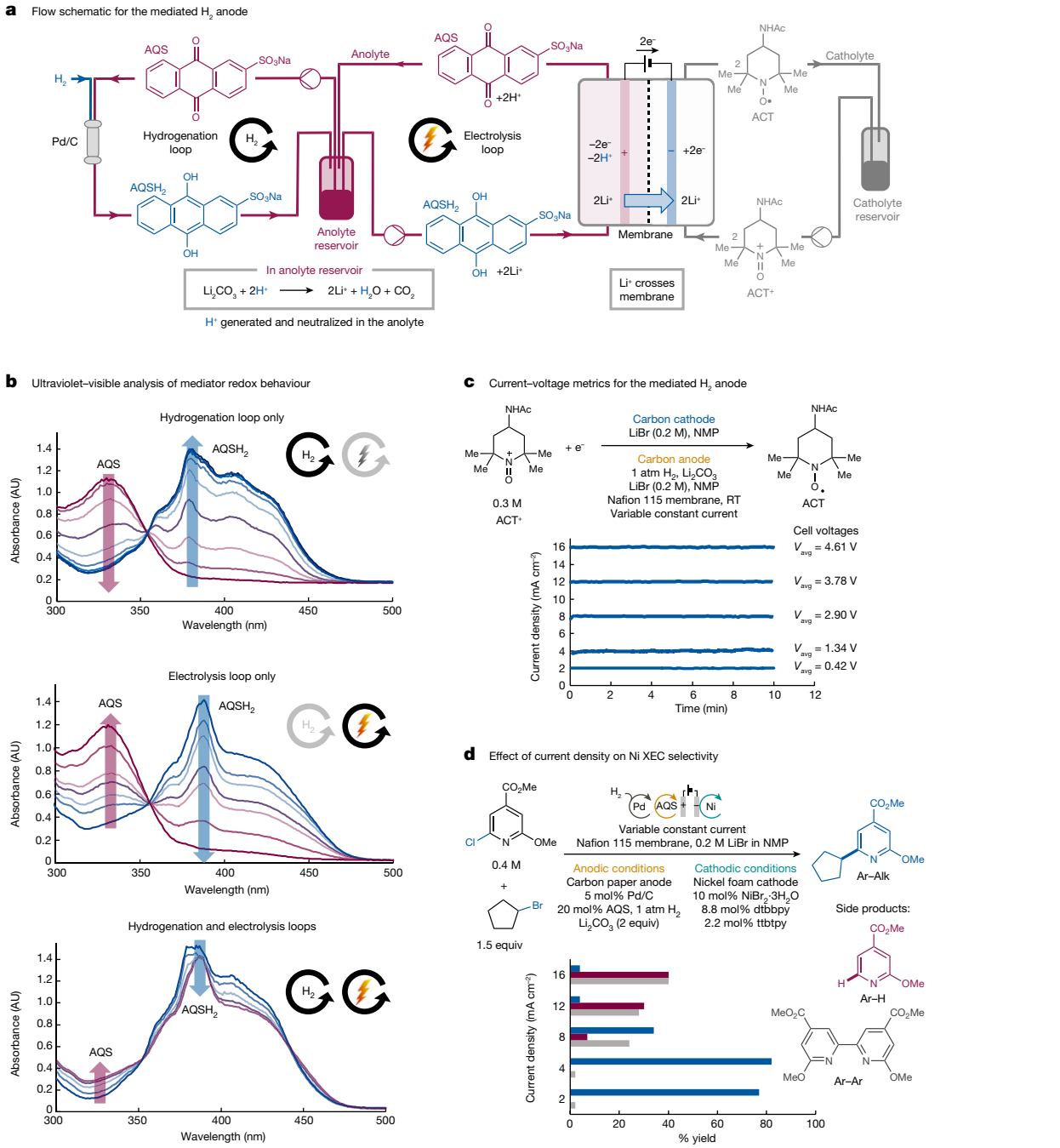

Fig. 3 | Quinone-mediated H_2 anode flow cell. a, Schematic diagram of the mediated H_2 anode flow system, integrating a hydrogenation loop with a packed-bed reactor for AQS hydrogenation and an electrolysis loop interfaced with a parallel-plate reactor for anodic oxidation of $AQSH_2$. **b**, Analysis of redox states of the quinone mediator in the anolyte reservoir, using in situ ultraviolet–visible spectroscopy, while circulating only through the hydrogenation loop, only through the electrolysis loop and through both the hydrogenation and the electrolysis loops. **c**, Operation of the mediated hydrogen anode shows stable cell voltage at current densities well beyond that needed to support Ni-catalysed XEC. **d**, Assessment of Ni XEC product selectivity at different current densities. Blue bars correspond to product formation, red bars correspond to formation of the Ar–H side product and grey bars correspond to formation of the biaryl side product. Optimal yield and selectivity are obtained at 4 mA cm^{-2}. AU, absorbance units; RT, room temperature.

of the hydrogenation loop without electrolysis leads to full reduction of the AQS to $AQSH_2$ (Fig. 3b, hydrogenation loop only), with an isosbestic point at 355 nm. Stopping flow in the hydrogenation loop and initiating the electrolysis loop while applying 5 mA current at the anode shows regeneration of AQS, while maintaining the isosbestic point (Fig. 3b, electrolysis loop only). When both loops are operating, the anolyte reservoir reaches a steady-state AQS/$AQSH_2$ ratio that reflects the balanced rates of the chemical and electrochemical reactions (85% $AQSH_2$ state of charge for the conditions shown in Fig. 3b, hydrogenation and electrolysis loops). Stable cell voltages were observed at current densities of 2–16 mA cm^{-2} (Fig. 3c), extending beyond the current densities determined to be necessary to support optimal performance of Ni-catalysed XEC at the cathode (Fig. 3d). Analysis of the yields and selectivities of the Ni-catalysed XEC reaction showed that optimal results with the indicated substrate were obtained at a current density of about 4 mA cm^{-2}.

The mediated H_2 anode was then evaluated in larger-scale applications of Ni-catalysed XEC using flow-electrolysis methods. A 5 cm^2

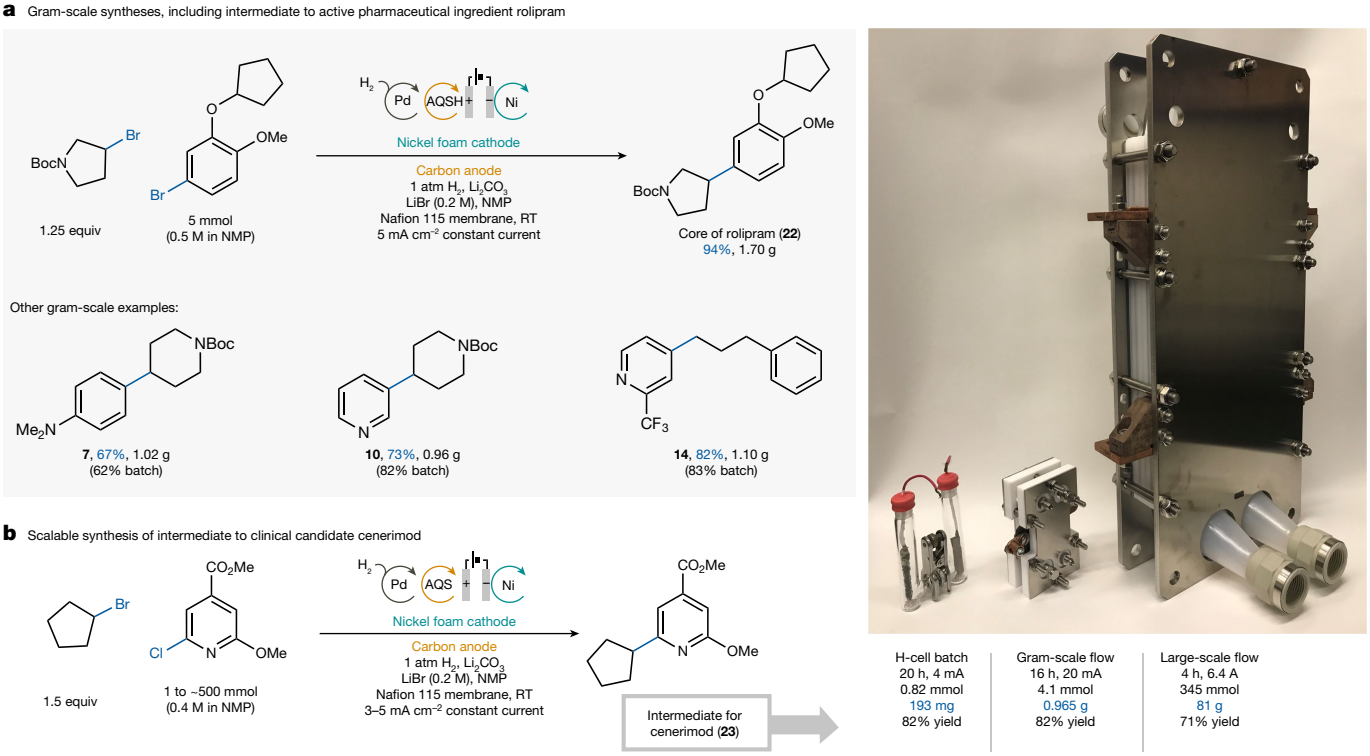

Fig. 4 | Scalable demonstration of the mediated H_2 anode to prepare molecules of pharmaceutical interest. a, Gram-scale Ni-catalysed XEC using a small parallel-plate flow reactor (5 cm^2 electrode surface area) to synthesize molecules, including an intermediate to the drug rolipram. **b**, Synthesis of an intermediate to the drug cenerimod in three different formats: an H-cell batch reactor, a small parallel-plate flow reactor (5 cm^2 electrode surface area) and a large parallel-plate flow reactor (1,600 cm^2 electrode surface area). See Methods for experimental details and the Supplementary Information for individual reaction conditions. RT, room temperature.

parallel-plate flow reactor was used to synthesize several compounds on the gram scale (Fig. 4a). The core structure of the antidepressant medication rolipram[36] was obtained in 94% isolated yield (1.70 g) using this method. Also, several candidates from batch screening were investigated, giving priority to examples previously shown to be challenging with a Ni-catalysed XEC process using sacrificial amine reductants (**7**, **10**, **14**)[29]. These gram-scale reactions proceeded in 15–30% higher yields than those obtained with the amine reductant and comparable yields to those obtained with a sacrificial Zn anode (see Extended Data Fig. 8). The origin of the improvement relative to the amine-based reductant was not examined; however, the positive results highlight the merits of this H_2-driven electrolysis method.

Gram-scale synthesis of an intermediate to the Phase III clinical candidate cenerimod[37] was similarly effective (Fig. 4b). An 82% product yield was obtained in a batch H-cell and no loss of yield was observed following transition to the gram-scale flow reactor. The flow conditions were then translated into a larger-scale commercial parallel-plate reactor that featured a stack of four membrane–electrode units with a total electrode surface area of 1,600 cm^2 (Extended Data Fig. 10). A current density of 4 mA cm^{-2} was retained in the larger reactor and the reaction proceeded at the 100 g scale with 71% yield (without optimization). The flow reactor applications show the stable operation of the H_2 anode and Ni XEC flow cell over 4–16 h of operation, and the total current of 6.4 A applied in the large-scale demonstration would be sufficient to deliver approximately 0.5 kg per day of the cross-coupled product.

Hydrogen represents an ideal, sustainable alternative to stoichiometric metal-based reductants, and the quinone-mediated H_2 anode system outlined herein establishes a unique strategy to use H_2 as the reductant for Ni XEC reactions. The quinone mediator is a versatile, electrochemically active hydrogen carrier. Pairing catalytic hydrogenation of the quinone with electrochemical oxidation of the hydroquinone enables efficient net electrochemical oxidation of hydrogen under non-aqueous conditions. The data presented above show how electrochemistry provides a means to amplify the reducing power of H_2, allowing H_2 to serve as a source of electrons even when it lacks the intrinsic chemical potential needed to generate highly reduced catalytic intermediates. The recirculating-flow mediated-anode system also offers unique flexibility in proton management that differs from other H_2 anodes, such as fuel-cell MEAs or gas-diffusion electrodes. Protons derived from hydroquinone oxidation are readily retained in the anode compartment, in which they can be neutralized and replaced with lithium ions, thereby allowing H_2 to serve as a proton-free source of electrons for the cathodic reaction. Each of these features has important implications for future development of H_2-driven electrosynthetic reduction reactions. Important opportunities include other reductive coupling reactions, such as those using various sp, sp^2 and sp^3 electrophiles; ketones, aldehydes and other carbonyl compounds; alkenes; and various small molecules, including CO_2 and SO_2 (ref. 38). Adaptations of this system may be considered that promote the transport of protons, rather than metal ions, through the membrane. Such extensions will provide the basis for electrochemical hydrogenation of organic molecules[5,39], including those proceeding by means of non-conventional mechanisms, such as the Birch reductions[40].

Online content

Any methods, additional references, Nature Portfolio reporting summaries, source data, extended data, supplementary information, acknowledgements, peer review information; details of author contributions and competing interests; and statements of data and code availability are available at https://doi.org/10.1038/s41586-023-06534-2.

1. Cardoso, D. S. P., Šljukić, B., Santos, D. M. F. & Sequeira, C. A. C. Organic electrosynthesis: from laboratorial practice to industrial applications. *Org. Process Res. Dev.* **21**, 1213–1226 (2017).
2. Pletcher, D. & Walsh, F. C. *Industrial Electrochemistry* 2nd edn, 298–311 (Kluwer, 1990).
3. Leech, M. C., Garcia, A. D., Petti, A., Dobbs, A. P. & Lam, K. Organic electrosynthesis: from academia to industry. *React. Chem. Eng.* **5**, 977–990 (2020).
4. Klein, M. & Waldvogel, S. R. Counter electrode reactions—important stumbling blocks on the way to a working electro-organic synthesis. *Angew. Chem. Int. Edn* **61**, e202204140 (2022).
5. Sherbo, R. S., Delima, R. S., Chiykowski, V. A., MacLeod, B. P. & Berlinguette, C. P. Complete electron economy by pairing electrolysis with hydrogenation. *Nat. Catal.* **1**, 501–507 (2018).
6. Danly, D. E. Development and commercialization of the Monsanto electrochemical adiponitrile process. *J. Electrochem. Soc.* **131**, 435C–442C (1984).
7. Barrette, W. C. & Sawyer, D. T. Determination of dissolved hydrogen and effects of media and electrode materials on the electrochemical oxidation of molecular hydrogen. *Anal. Chem.* **56**, 653–657 (1984).
8. Ledezma-Yanez, I., Díaz-Morales, O., Figueiredo, M. C. & Koper, M. T. M. Hydrogen oxidation and hydrogen evolution on a platinum electrode in acetonitrile. *ChemElectroChem.* **2**, 1612–1622 (2015).
9. Lazouski, N., Chung, M., Williams, K., Gala, M. L. & Manthiram, K. Non-aqueous gas diffusion electrodes for rapid ammonia synthesis from nitrogen and water-splitting-derived hydrogen. *Nat. Catal.* **3**, 463–469 (2020).
10. Suryanto, B. H. R. et al. Nitrogen reduction to ammonia at high efficiency and rates based on a phosphonium proton shuttle. *Science* **372**, 1187–1191 (2021).
11. Hodgetts, R. Y., Du, H.-L., Nguyen, T. D., MacFarlane, D. & Simonov, A. N. Electrocatalytic oxidation of hydrogen as an anode reaction for the Li-mediated N_2 reduction to ammonia. *ACS Catal.* **12**, 5231–5246 (2022).
12. Fu, X. et al. Continuous-flow electrosynthesis of ammonia by nitrogen reduction and hydrogen oxidation. *Science* **379**, 707–712 (2023).
13. Goldfogel, M. J., Huang, L. & Weix, D. J. in *Nickel Catalysis in Organic Synthesis* (ed. Ogoshi, S.) 183–222 (Wiley, 2020).
14. Nimmagadda, S. K. et al. Development and execution of an Ni(II)-catalyzed reductive cross-coupling of substituted 2-chloropyridine and ethyl 3-chloropropanoate. *Org. Process Res. Dev.* **24**, 1141–1148 (2020).
15. Beutner, G. L. et al. A process chemistry benchmark for sp^2–sp^3 cross couplings. *J. Org. Chem.* **86**, 10380–10396 (2021).
16. Moulik, S., Vaishnavi, B. A., Nagar, H. & Sridhar, S. in *Encyclopedia of Membranes* (eds Drioli, E. & Giorno, L.) 1973–1983 (Springer, 2016).
17. Goor, G., Glenneberg, J., Jacobi, S., Dadabhoy, J., & Candido, E. in *Ullmann's Encyclopedia of Industrial Chemistry* (Wiley, 2019).
18. Huskinson, B. et al. A metal-free organic–inorganic aqueous flow battery. *Nature* **505**, 195–198 (2014).
19. Kwabi, D. G., Ji, Y. & Aziz, M. J. Electrolyte lifetime in aqueous organic redox flow batteries: a critical review. *Chem. Rev.* **120**, 6467–6489 (2020).
20. Anson, C. W. & Stahl, S. S. Mediated fuel cells: soluble redox mediators and their applications to electrochemical reduction of O_2 and oxidation of H_2, alcohols, biomass, and complex fuels. *Chem. Rev.* **120**, 3749–3786 (2020).
21. Acemoglu, M., Baenziger, M., Krell, C. M. & Marterer, W. in *Transition Metal-Catalyzed Couplings in Process Chemistry* (eds Magano, J. & Dunetz, J. R.) 15–23 (Wiley, 2013).
22. Jennings, P. W., Pillsbury, D. G., Hall, J. L. & Brice, V. T. Carbon-carbon bond formation via organometallic electrochemistry. *J. Org. Chem.* **41**, 719–722 (1976).
23. Conan, A., Sibille, S., d'Incan, E. & Périchon, J. Nickel-catalysed electroreductive coupling of α-halogenoesters with aryl or vinyl halides. *J. Chem. Soc. Chem. Commun.* 48–49 (1990).
24. Perkins, R. J., Pedro, D. J. & Hansen, E. C. Electrochemical nickel catalysis for sp^2-sp^3 cross-electrophile coupling reactions of unactivated alkyl halides. *Org. Lett.* **19**, 3755–3758 (2017).
25. Li, H. et al. Ni-catalyzed electrochemical decarboxylative C–C couplings in batch and continuous flow. *Org. Lett.* **20**, 1338–1341 (2018).
26. Perkins, R. J., Hughes, A. J., Weix, D. J. & Hansen, E. C. Metal-reductant-free electrochemical nickel-catalyzed couplings of aryl and alkyl bromides in acetonitrile. *Org. Process Res. Dev.* **23**, 1746–1751 (2019).
27. DeLano, T. J. & Reisman, S. E. Enantioselective electroreductive coupling of alkenyl and benzyl halides via nickel catalysis. *ACS Catal.* **9**, 6751–6754 (2019).
28. Jiao, K.-J. et al. Nickel-catalyzed electrochemical reductive relay cross-coupling of alkyl halides to aryl halides. *Angew. Chem. Int. Edn* **132**, 6520–6524 (2020).
29. Franke, M. C. et al. Zinc-free, scalable reductive cross-electrophile coupling driven by electrochemistry in an undivided cell. *ACS Catal.* **12**, 12617–12626 (2022).
30. Harwood, S. J. et al. Modular terpene synthesis enabled by mild electrochemical couplings. *Science* **375**, 745–752 (2022).
31. Hamby, T. B., LaLama, M. J. & Sevov, C. S. Controlling Ni redox states by dynamic ligand exchange for electroreductive Csp^3–Csp^2 coupling. *Science* **376**, 410–416 (2022).
32. Sanfilippo, D. & Rylander, P. N. Hydrogenation and dehydrogenation. *Ullmann's Encyclopedia of Industrial Chemistry* (Wiley, 2009).
33. Everson, D. A., Shrestha, R. & Weix, D. J. Nickel-catalyzed reductive cross-coupling of aryl halides with alkyl halides. *J. Am. Chem. Soc.* **132**, 920–921 (2010).
34. Preger, Y. et al. Quinone-mediated electrochemical O_2 reduction accessing high power density with an off-electrode Co-N/C catalyst. *Joule* **2**, 2722–2731 (2018).
35. Preger, Y. et al. Anthraquinone-mediated fuel cell anode with an off-electrode heterogeneous catalyst accessing high power density when paired with a mediated cathode. *ACS Energy Lett.* **5**, 1407–1412 (2020).
36. Zhu, J., Mix, E. & Winblad, B. The antidepressant and antiinflammatory effects of rolipram in the central nervous system. *CNS Drug Rev.* **7**, 387–398 (2001).
37. Piali, L. et al. Cenerimod, a novel selective $S1P_1$ receptor modulator with unique signaling properties. *Pharmacol. Res. Perspect.* **5**, e00370 (2017).
38. Liu, Y., Li, P., Wang, Y. & Qiu, Y. Electroreductive cross-electrophile coupling (eXEC) reactions. *Angew. Chem. Int. Edn* **62**, e202306679 (2023).
39. Yang, J., Qin, H., Yan, K., Cheng, X. & Wen, J. Advances in electrochemical hydrogenation since 2010. *Adv. Synth. Catal.* **363**, 5407–5416 (2021).
40. Peters, B. K. et al. Scalable and safe synthetic organic electroreduction inspired by Li-ion battery chemistry. *Science* **363**, 838–845 (2019).

Methods

Electrochemical potential benchmarking

The H^+/H_2 reduction potential was characterized through both OCP and CV analysis (Extended Data Fig. 1a). CV analysis took place over a very narrow potential window centred around the OCP and served to allow for calculation of a zero-point potential (E_z), the averaged potentials at which the voltammogram reached zero current on its oxidative (E_a) and reductive (E_c) sweeps ($E_z = (E_a + E_c)/2$). This complementary analytical approach, reported in a recent study[41], validated the OCP measurements and confirmed that the solution was electrochemically well poised. All measurements were conducted using a Pt coil working electrode, platinum wire counter electrode and a Ag/Ag^+ reference electrode composed of a Ag wire in 0.1 M $AgNO_3$ in NMP containing 0.1 M tetrabutylammonium hexafluorophosphate (NBu_4PF_6), with the latter then calibrated to $Fc^{+/0}$ at a 3-mm-diameter glassy carbon working electrode. The Pt coil was pretreated by electrolysis at +1.5 V and −0.25 V versus Ag/AgCl in 1 M aqueous H_2SO_4 immediately before OCP measurements. Data were collected using a solution of 0.1 M CF_3SO_3H (proton source) and 0.1 M NBu_4PF_6 (supporting electrolyte) in NMP under an atmosphere of H_2. CV analysis was conducted at a scan rate of 10 mV s^{-1}.

CV analysis was also used to determine the reduction potential and electrochemical reversibility of AQS and the Ni catalyst species used for XEC (Extended Data Fig. 1b and Fig. 1c). CV data for AQS was collected as follows: to a glass CV reaction vessel fitted with a cross-shaped stir bar was added AQS (31.0 mg, 0.1 mmol), triflic acid (0.09 ml, 1 mmol) and 10 ml of 0.1 M NBu_4PF_6 in NMP solution. The vessel was then sealed with a cap fitted with a 3-mm-diameter glassy carbon working electrode, Pt wire counter electrode and a Ag/Ag^+ reference electrode. N_2 was bubbled through the solution for 20 min to degas the solution and cell. At this point, the gas stream was pulled above the solvent line, the solution was allowed to become quiescent for 2 min and a cyclic voltammogram was collected. For the Ni catalysts, CV analysis was conducted on a 0.01-M Ni/ligand solution in NMP with 0.1 M LiBr as the supporting electrolyte. Catalysts were formed by pre-stirring 1:1 solution of the Ni salt and the ligand of interest. CV was conducted with a glassy carbon working electrode and platinum wire counter electrode. A Ag/Ag^+ reference electrode was used, calibrated to $Fc^{+/0}$. A scan rate of 100 mV s^{-1} was used for these experiments.

General procedures for mediated H_2 anode enabled XEC

Divided H-cell. In a nitrogen-filled glovebox, to a 6-dram vial fitted with a cross-shaped stir bar and a Teflon-lined cap was added LiBr (347 mg, 4.00 mmol) and NMP (20 ml) to generate a 0.2-M LiBr in NMP electrolyte solution. The mixture was stirred in a glovebox until complete dissolution of the LiBr. This vial was then removed from the glovebox and placed under positive pressure of nitrogen on a Schlenk line. A 2.5 × 2.5-cm square of Nafion 115 was cut and placed in a small beaker. A 1 ml aliquot of the 0.2 M LiBr solution was removed under positive pressure of nitrogen and used to soak the Nafion membrane for 10 min. A divided H-cell was then assembled around the Nafion membrane using a Viton O-ring and ring clamp to secure the cell. Each chamber of the cell was fitted with a cross-shaped stir bar. To the anodic chamber was added 5 wt% palladium on carbon (42 mg, 0.020 mmol, 2 mol%), AQS (62 mg, 0.19 mmol, 20 mol%) and Na_2CO_3 (210 mg, 2 mmol, 2 equiv). A 5 × 1 × 0.5 cm rectangle of reticulated vitreous carbon (RVC) was cut using a razor blade and affixed to copper wire. A 14/20 rubber septum was punctured with a 14-gauge needle and the copper wire (with RVC electrode) was threaded through the rubber septum before removal of the needle. The RVC electrode was then placed in the anodic chamber roughly 5 mm above the stir bar and the 14/20 joint sealed with the rubber septum.

To the cathodic chamber was added $NiBr_2 \cdot 3H_2O$ (27.3 mg, 0.105 mmol, 10 mol%), dtbbpy (23.6 mg, 0.088 mmol, 8.8 mol%) and ttbtpy (8.8 mg, 0.022 mmol, 2.2 mol%). At this stage, if the aryl halide or alkyl halide coupling partners were solid, they were added to the cathodic compartment. A 2 × 4-cm rectangle of nickel foam was cut and affixed to copper wire (folded over the wire and crimped with a pair of pliers). A 14/20 rubber septum was punctured with a 14-gauge needle and the copper wire (with nickel foam electrode) was threaded through the rubber septum before removal of the needle. The nickel foam electrode was then placed in the cathodic chamber roughly 5 mm above the stir bar and the 14/20 joint sealed with the rubber septum. The headspace of the chamber of the H-cell was cleared by means of nitrogen flush for 10 min. The anodic compartment headspace was then cleared with hydrogen gas for 10 min. The electrolyte solution was withdrawn using a syringe; 5 ml was added to the cathodic compartment under nitrogen atmosphere and 7.5 ml was added to the anodic compartment. The hydrogen purge needle was submerged under the surface of the solution and the hydrogen flow rate adjusted to provide roughly one bubble per second. The anolyte and catholyte were stirred at 600 rpm until complete dissolution of the catholyte. At this stage, if the aryl or alkyl halide electrophile were a liquid, they were added to the cathodic compartment with the use of a Hamilton syringe. The copper wires were attached to a BASi Epsilon or CH Instruments potentiostat with the cathode identified as the working electrode and the anode as the counter and reference electrode. Constant-current electrolysis was performed at −3 to −4 mA until the passage of 3.5 F mol^{-1} or until the cell potential reached −10 V.

On completion of the reaction, the catholyte was either isolated (for substrate scope experiments, as in Fig. 2) or an aliquot was collected for determination of an analytical yield (during optimization; see Extended Data Fig. 3 and the tables in the Supplementary Information). Isolation: catholyte was collected and concentrated under reduced pressure to dryness. The resultant residue was dissolved in EtOAc and passed through a small plug of silica to remove metal salts, concentrated under reduced pressure to dryness and purified by silica gel chromatography. Yields were calculated by mass of isolated product, accounting for notable remaining impurities. Analytical yield: catholyte was transferred using an Eppendorf pipette to a 4-dram vial. The cathode and cathode chamber were rinsed with acetonitrile (MeCN) and these rinsings were transferred to the vial. 1,3,5-Trimethoxybenzene (84 mg, 0.5 mmol, 0.5 equiv) was added to the vial as internal standard. Either a 2-µl aliquot was removed and diluted into a 200-µl 3:1 (v/v) mixture of MeCN/dimethyl sulfoxide for ultra-performance liquid chromatography-mass spectrometry (UPLC-MS) analysis or a 50-µl aliquot was removed and diluted into 500 µl of MeCN-d_3 for ^1H NMR analysis. A 400-MHz NMR spectrometer was used with a d1 value of 6 s with 32 scans.

Divided gram-scale flow cell. An ElectroCell Micro Flow Cell (Extended Data Figs. 4 and 7a) was used as the flow apparatus. The flow cell consisted of a Nafion 115 cation-exchange membrane, a 5-cm^2 carbon paper anode distanced from the membrane with a polytetrafluoroethylene (PTFE) screen, a 5-cm^2 commercial nickel foam cathode directly against the membrane and two PTFE flow frames, with incompressible components separated by Viton gaskets.

The packed-bed hydrogenation reactor (2.2 in. length, 0.5 in. OD) was made from a stainless-steel (SS) tube with 5 wt% Pd/C (23 mg, 0.01 mmol, 1 mol%), retained using 1 in. of glass wool on each end. The anolyte solution, catholyte solution and catalytic packed bed were prepared before the operation. Two 24/40 rubber septa were punctured with a 14-gauge needle and Teflon tubing (1/8 in. ID and 3/16 in. OD) was threaded through the septa. This Teflon tubing was fitted with 20 µm high-performance liquid chromatography (HPLC) frits (Analytical Sales, product number 49225A). To a 100-ml three-neck 24/40 round-bottom flask with an oval stir bar was added AQS (78 mg, 0.25 mmol, 5 mol%) and Li_2CO_3 (554 mg, 7.50 mmol, 1.5 equiv). Two of the openings were fitted with the septa fitted with the frits and the final opening was fitted with an unmodified 24/40 rubber septum. The flask was then transferred into a nitrogen-filled glovebox and LiBr (1.042 g,

12.00 mmol) and NMP (60 ml) were added and the heterogeneous mixture was stirred for 20 min. The flask was removed from the glovebox and placed under nitrogen atmosphere on a Schlenk line for 10 min. The Teflon tubing outlets were attached to size 14 Masterflex PharMed BPT tubing connected to the packed-bed reactor (with HPLC pump) and flow cell (with peristaltic pump). H_2 gas was then vigorously bubbled through a 22-gauge needle into the solution to allow for hydrogen saturation of the solution. To a 8-dram vial fitted with a cross-shaped stir bar was added $NiBr_2{\cdot}3H_2O$ (136 mg, 10 mol%, 0.5 mmol), dtbbpy (118 mg, 8.8 mol%, 0.44 mmol) and ttbtpy (44.2 mg, 2.2 mol%, 0.11 mmol). At this stage, if the alkyl or aryl electrophile were solid, they were added to the vessel. The vial was then transferred to a nitrogen-filled glovebox and LiBr (0.208 g, 2.4 mmol, 0.48 equiv) and NMP (12 ml) were added. The catholyte-containing vial was then stirred for 10 min. The sealed vial was then removed from the glovebox and placed under nitrogen atmosphere on a Schlenk line. Size 14 Masterflex PharMed BPT tubing connected to the cathodic side of the Micro Flow Cell was fed into the cathodic reservoir by means of a 16-gauge needle (with peristaltic pump). The system was left to equilibrate under nitrogen/hydrogen purge for 10 min. In one flow loop, a HPLC pump flowed the anolyte at 4 ml min^{-1} through the Teflon tubing and into the catalytic packed-bed reactor. In the catalytic reactor, the AQS was reduced to $AQSH_2$ and the anolyte then flowed back into the reservoir. After 45 min, a second flow loop, which used a peristaltic pump to cycle anolyte and catholyte through the electrochemical flow cell, was started. There the $AQSH_2$ was oxidized on the carbon anode to form AQS and protons. The protons, separated from the proton-exchange membrane by a PTFE screen, were carried back into the reservoir. Protons were prevented from accumulating by reaction with Li_2CO_3 in the anodic reservoir. On the cathode, Ni-catalysed reductive coupling was expected to take place.

The flow cell was connected to a BioLogic BP-300 potentiostat with the cathode selected as the working electrode and the anode as the counter electrode. A chronopotentiometry experiment was conducted with a constant current of −20 mA (current density = 4 mA cm^{-2}) until 3.5 F mol^{-1} were passed or until the cell potential dropped below −8 V. Initial cell voltages were reasonably constant, averaging −1.99 V with a standard deviation of 0.045 V over four replications of the cenerimod intermediate synthesis. On completion of electrolysis, the catholyte was collected and concentrated to dryness under high vacuum. The resultant residue was dissolved in EtOAc and passed through a small plug of silica to remove metal salts, concentrated to dryness and purified by silica gel chromatography.

This approach was used to synthesize several Ni XEC products on the gram scale. The API intermediates for rolipram and cenerimod were isolated and the figure reflects the isolated yield. Replicating the synthesis of the cenerimod intermediate four times yielded an average (analytical) yield of 82.7 ± 4.8%. The corresponding faradaic efficiency for these reactions averaged 84.9 ± 3.1%. Compounds **7** and **10** were characterized by UPLC-MS, with yields obtained through the use of an external standard calibration curve using authentic product. Compound **14** reports an assay yield using ^{19}F NMR with C_6F_6 as an internal standard.

Divided large-scale flow cell. An electrochemical flow cell (the Electro Syn Cell from ElectroCell A/S) was used as the flow apparatus (Extended Data Fig. 10a). The flow cell consisted of a Nafion 117 cation-exchange membrane, a 0.16 m^2 carbon felt on graphite anode distanced from the membrane with a PTFE screen, a 0.16 m^2 commercial nickel foam cathode directly against the membrane and two polypropylene flow frames, with incompressible components separated by PTFE gaskets.

The anodic solution was prepared in a nitrogen-filled glovebox by weighing AQS into an 8-dram vial (7.69 g, 24.8 mmol, 5 mol%) and LiBr into two 8-dram vials (2 × 52-g vials = 104 g, 1,200 mmol, 2.4 equiv). In a nitrogen-filled glovebox, lithium carbonate (55 g, 744 mol, 1.5 equiv) was weighed into a 500-ml Nalgene container. AQS and one vial of LiBr were added to a 1-l Nalgene bottle fitted with a cross-shaped stir bar inside the glovebox. To a second 1-l Nalgene bottle fitted with a cross-shaped stir bar was added the second vial of LiBr. To each of the Nalgene bottles was added approximately 750 ml of anhydrous NMP from 2 × 1-l bottles. Each Nalgene bottle was mixed using rotary stirring for 1 h. On the day of reaction, the bottles were then removed from the glovebox, the stir bar was removed and the contents were charged to the anolyte reservoir (12-l round-bottom flask). The bottle was rinsed with the remaining NMP (approximately 250 ml NMP per bottle). Further dry NMP (1 l) was used to rinse the two Nalgene bottles. Lithium carbonate was added into the anodic reservoir to avoid accumulation of generated protons in solution. To retain the lithium carbonate, it was packaged into seven pouches made of filter paper sealed with polypropylene zip ties (approx. 7.9 g per pouch) for a total of 55 g of lithium carbonate charged. Finally, 3 l of NMP were added to the anolyte reservoir to bring the total volume to 6 l. The headspace was purged with N_2, maintaining a vessel pressure below 5 psi.

The cathodic solution was prepared in a nitrogen glovebox. To separate 8-dram vials was weighed $NiBr_2{\cdot}$glyme (1,2-dimethoxyethane)nickel dibromide (15.31 g, 49.6 mmol, 10 mol%), dtbbpy (8.79 g, 32.7 mmol, 6.6 mol%), ttbtpy (8.76 g, 21.82 mmol, 4.4 mol%) and LiBr (52.1 g, 600 mmol, 1.2 equiv). These solids were transferred to a 1-l Nalgene bottle fitted with a cross-shaped stir bar followed by 0.5 l of dry NMP. Methyl 2-chloro-6-methoxyisonicotinate (100 g, 496 mmol) was weighed into a 500-ml Nalgene bottle and then transferred into a second 1-l Nalgene bottle containing a stir bar inside the glovebox followed by 0.5 l of dry NMP. The contents of each were mixed using rotary stirring overnight, after which they were partially dissolved but not entirely homogeneous. On the day of the flow experiment, stir bars were removed and both solutions were charged to the catholyte reservoir (a 10-litres glass vessel) and every bottle was rinsed with 2 × 0.5 l NMP. Then a solution of cyclopentyl bromide (111 g, 80 ml, 744 mmol, 1.5 equiv) in 0.25 l of NMP was added. Finally, 0.75 l of dry NMP was added to the reservoir to achieve the desired 3-l volume. The headspace was swept with N_2 (maintaining a vessel pressure below 5 psi) and the catholyte was mixed with overhead stirring for more than 1 h (40 rpm); as a result, a homogeneous mixture was obtained and overhead stirring was stopped.

The packed-bed hydrogenation reactor was composed of a Pd bed in a cylindrical SS reactor. The SS reactor (0.5 in. OD, 9.5 in. height) was packed with 3 g of dry Pd/C (Evonik 5 wt%, lot no. PMPC150388, catalyst type PMPC SP1010D, 1.4 mmol, 0.3 mol%) and secured with two SS disk frits (304 SS, 40 mesh). The Pd column was rinsed with NMP without a return line to the anolyte reservoir to remove any loose particulates and then the column outlet was plumbed into the anolyte reservoir return loop. All NMP was removed from both the anolyte and catholyte reservoirs and then Karl Fischer titrations were performed to assess water content before charging reagents. (KF anolyte = 2 measurements: 4,558 ppm, 4,582 ppm; KF catholyte = 2 measurements: 1,486 ppm, 1,455 ppm.) Anolyte and catholyte solutions were then charged and brought to the desired final volume (6 l anolyte, 3 l catholyte).

The fully composed flow system (Extended Data Fig. 9) was then used to perform a Ni XEC reaction on scale. Anolyte and catholyte solutions were pumped between the bed and the reservoir using a Masterflex Digital Gear Pump with pump head N25, whereas an N21 pump head was used for the hydrogenation reactor loop. Before electrolysis, the anolyte solution was pumped through the hydrogenation reactor at a rate of 0.5 l min^{-1} in co-flow with H_2 gas, which was controlled by an Alicat mass flow controller at 70 SCCM (roughly 70 cm^3 min^{-1}). The anolyte solution transitioned from yellow (fully oxidized) to green (partially or fully reduced). Any unreacted hydrogen flowed into the anolyte reservoir and combined with a N_2 sweep to achieve a diluted, non-flammable gas mixture that was vented to exhaust. After pre-reduction of the anthraquinone species, the anolyte and catholyte were circulated through the cell at rates of 4.0 l min^{-1} and a power supply was used to apply 6.4 A of constant current.

The reaction was monitored with analysis of cathodic aliquots by UPLC analysis every 20–30 min (Extended Data Fig. 10b) and the liquid chromatography area percent (LCAP) of the substrate and product were used to roughly monitor the degree of the reaction. When the reaction reached the cutoff cell voltage of 3 V after just under 4 h, the experiment was stopped. The final product assay was conducted by quantitative ^{1}H NMR in triplicate and showed 72% assay yield.

Mediated-anode benchmarking using a Bobbitt's salt cathode

A modified version of the divided gram-scale flow cell was also used for benchmarking of the mediated hydrogen anode with a Bobbitt's salt cathode. Typically, these data were collected while maximizing parameters that would enable maximum attainable currents. Alterations to that end were as follows: a 5-cm^2 carbon paper cathode was used, distanced from the membrane with a PTFE screen; the concentration of AQS in the anolyte was 0.3 M (5.58 g, 16.9 mmol) with 0.4 M NBu_4BF_4 (7.9 g, 24 mmol 0.4 M) as the supporting electrolyte, in 60 ml NMP (near the solubility limit of AQS in NMP), with a large excess of Li_2CO_3 supplied for the purpose of the experiment; the packed-bed hydrogenation reactor used 5 wt% Pd/C (50 mg, 0.023 mmol); the catholyte consisted of 0.6 M Bobbitt's salt (4-acetamido-2,2,6,6-tetramethylpiperidine-1-oxyl tetrafluoroborate, 3.6 g, 12 mmol) and 0.4 M NBu_4BF_4 (2.63 g, 7.99 mmol) as the supporting electrolyte in 20 ml NMP, matching the faradaic capacity of the two solutions. The flow rate through the cell was 80 ml min^{-1}.

Data availability

The NMR spectra for characterized compounds are available in the data repository at https://doi.org/10.6084/m9.figshare.23511828. The authors declare that all other data supporting the findings of this study are available in the paper and its Supplementary Information files.

41. Zamora Zeledón, J. A., Jackson, A., Stevens, M. B., Kamat, G. A. & Jaramillo, T. F. Methods—a practical approach to the reversible hydrogen electrode scale. *J. Electrochem. Soc.* **169**, 066505 (2022).

Acknowledgements The authors thank B. Armstrong (EPSE) and C. Nietupski (HPL) of Merck & Co., Inc. for valuable discussions, feedback and assistance in performing the large-scale implementation of this chemistry. The authors thank C. Salazar of UW-Madison for assistance with gas-uptake experiments and A. M. Norris and M. Boasso of Merck & Co., Inc. for assistance in the preparation of Extended Data Fig. 4. Financial support for development of the mediated H_2 anode was provided by the Center for Molecular Electrocatalysis, an Energy Frontier Research Center, funded by the U.S. Department of Energy, Office of Science, Office of Basic Energy Sciences and Merck Sharp & Dohme LLC, a subsidiary of Merck & Co., Inc. The development of Ni-catalysed XEC reactions and their integration with the mediated H_2 anode was supported by the NSF (PFI-RP 2122596). Spectroscopic instrumentation was partially supported by the NIH (1S10 OD020022-1) and the NSF (CHE-1048642).

Author contributions S.S.S., J.B.G., J.T. and M.R.J. were involved in conceptualization of the project. Lab-scale efforts were conducted by M.R.J., J.T., V.S., M.C.F., J.B.G., S.M.M.K. and L.W. Large-scale efforts were conducted by C.B., D.L., F.L., T.P.V., M.D.W., J.T. and M.R.J. This project was completed under the supervision of S.S.S., T.W.R. and D.J.W. and supported by funding acquired by S.S.S., T.W.R., D.J.W., C.M.H. and N.A.S. Manuscript writing was led by S.S.S., M.R.J. and J.T., with contributions from all authors.

Competing interests A patent application describing a mediated H_2 anode has been filed.

Additional information
Supplementary information The online version contains supplementary material available at https://doi.org/10.1038/s41586-023-06534-2.
Correspondence and requests for materials should be addressed to Daniel J. Weix, Thatcher W. Root or Shannon S. Stahl.
Peer review information *Nature* thanks Alastair Lennox and the other, anonymous, reviewer(s) for their contribution to the peer review of this work.

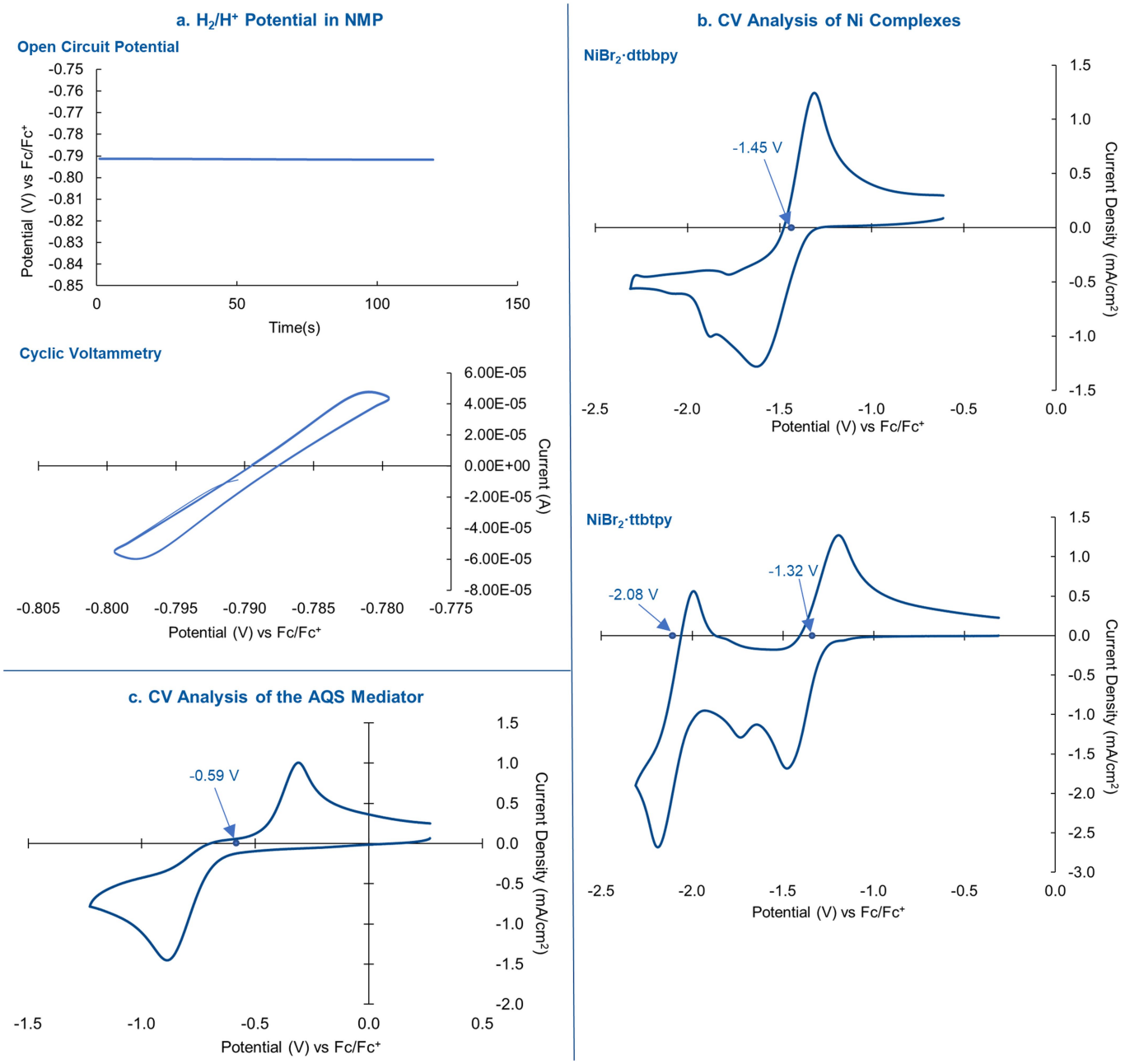

Extended Data Fig. 1 | Electrochemical reduction potential measurements. CV and OCP measurements were performed using a glassy carbon (CV) or Pt (OCP) working electrode and a platinum wire counter electrode, with CV scan rates of 10 mV s^{-1} (panel **a**) or 100 mV s^{-1} (panels **b** and **c**). A Ag/Ag^+ reference electrode was used and calibrated to $Fc^{+/0}$. **a**, H_2/H^+ OCP data showing a stable potential of −0.79 V versus $Fc^{+/0}$ and complementary CV analysis, conducted at a scan rate of 10 mV s^{-1}, showing a zero-point potential at −0.79 V versus $Fc^{+/0}$. Data were collected using a solution of 0.1 M CF_3SO_3H (proton source) and 0.1 M NBu_4PF_6 (supporting electrolyte) in NMP under 1 atm of H_2. **b**, CV data for 0.01 M Ni/ligand (1:1) solutions in NMP with 0.1 M LiBr as the supporting electrolyte. $NiBr_2$·dtbbpy shows a single clear redox feature corresponding to a Ni^{II}/Ni^0 transition; $NiBr_2$·ttbtpy shows two redox features: a higher-potential feature corresponding to Ni^{II}/Ni^{I} and a lower-potential feature corresponding to Ni^{I}/Ni^0. Ni/ligand solutions often generate mixtures of different species and the precise speciation was not investigated or explained to identify the origin of the smaller CV peaks present in these scans. **c**, CV analysis of a 0.01-M AQS solution in NMP. 0.1 M CF_3SO_3H proton source, N_2 atmosphere, 0.1 M NBu_4PF_6.

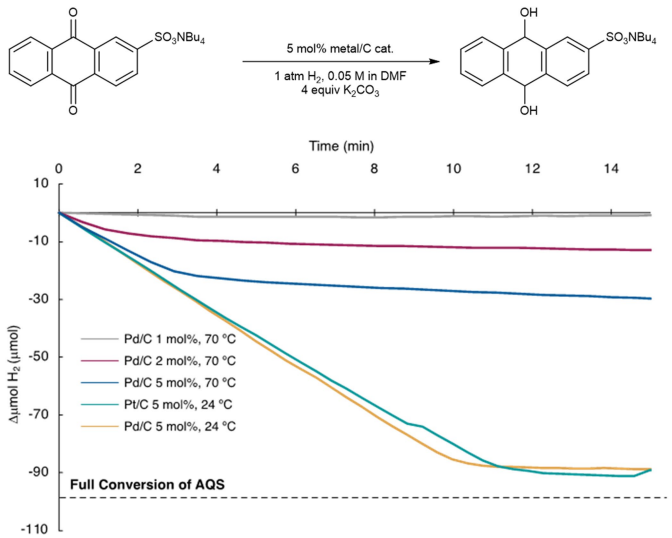

Extended Data Fig. 2 | Reduction of AQS on carbon-supported Pt and Pd catalysts at 24 °C and 70 °C under 1 atm H_2. Theoretical full substrate conversion corresponds to 100 µmol of consumed H_2. Both Pd/C and Pt/C catalysts demonstrated rapid rates of AQS hydrogenation, achieving quasi-complete conversion within 15 min. Pd/C was selected owing to its lower cost. At higher temperatures, although the initial rate remained unchanged, reactivity stopped before complete substrate reduction and reduction of the catalyst loading showed progressively earlier cessation of hydrogen consumption. These data suggest that the catalyst tolerates the AQS solution at room temperature but that it deactivates at elevated temperature. The reactor bed was operated at room temperature.

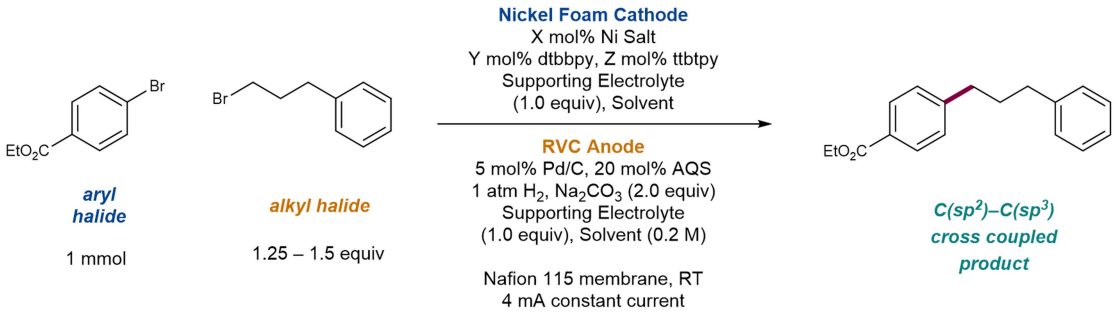

nickel (mol%)	dtbbpy (mol %)	ttbtpy (mol %)	solvent	supporting electrolyte	conc.	AlkBr loading	% Yield[a] ArBr	ArH	Ar_2	AlkBr	AlkH	Alk_2	AlkAr
10	20	0	DMF	NBu_4PF_6	0.2 M	1.5 equiv	0	2	41	2	16	48	31
10	11	0	DMF	NBu_4PF_6	0.2 M	1.5 equiv	0	2	81	127	0	0	16
10	11	0	DMF	$NaClO_4$	0.2 M	1.5 equiv	5	4	88	133	0	5	2
10	11	0	DMF	LiBr	0.2 M	1.5 equiv	3	3	86	142	0	0	6
10	8.8	2.2	DMF	NBu_4PF_6	0.2 M	1.5 equiv	0	17	26	71	25	5	53
10	5.5	5.5	DMF	NBu_4PF_6	0.2 M	1.5 equiv	0	34	5	4	5	50	57
10	8.8	2.2	DMA	NBu_4PF_6	0.2 M	1.5 equiv	0	13	10	52	23	11	73
10	8.8	2.2	NMP	NBu_4PF_6	0.2 M	1.5 equiv	0	4	6	11	15	41	88
5	4.4	1.1	NMP	NBu_4PF_6	0.2 M	1.5 equiv	0	7	10	10	3	4	73
2.5	2.2	0.55	NMP	NBu_4PF_6	0.2 M	1.5 equiv	23	9	64	44	4	5	6
10	8.8	2.2	NMP	LiBr	0.2 M	1.0 equiv	0	4	13	4	7	13	81
10	8.8	2.2	NMP	LiBr	0.4 M	1.25 equiv	3	2	1	0	0	17	78
10	8.8	2.2	NMP	LiBr	0.6 M	1.25 equiv	0	1	4	0	0	28	84
10[b]	8.8	2.2	NMP	LiBr	0.2 M	1.25 equiv	0	0	8	3	5	13	82
10[b]	8.8	2.2	NMP	$NaPF_6$	0.2 M	1.25 equiv	80	0	4	110	0	0	<5
10[b]	8.8	2.2	NMP	$NaClO_4$	0.2 M	1.25 equiv	74	7	6	100	0	4	<5

[a] Yield determined by calibrated UPLC analysis at 210.5 nm with 1,3,5-trimethoxybenzene as internal standard.
[b] Reaction performed with $NiBr_2 \cdot 3H_2O$.

Extended Data Fig. 3 | Optimization of mediated H_2 anode conditions for Ni XEC. Screening on mg scale in an H-cell identified advantageous reaction conditions (top table), including choice of polar aprotic solvent (NMP), supporting electrolyte (LiBr) and substrate ratio (1:1.25 Ar:Alk). An optimal catalyst composition of 8.8 mol% dtbbpy and 2.2 mol% ttbtpy with 10 mol% $NiBr_2 \cdot 3H_2O$ was identified for aryl bromides. DMA, *N*,*N*-dimethylacetamide.

a. Flow Cell Schematic for H_2 Anode Benchmarking with Bobbitt's Salt

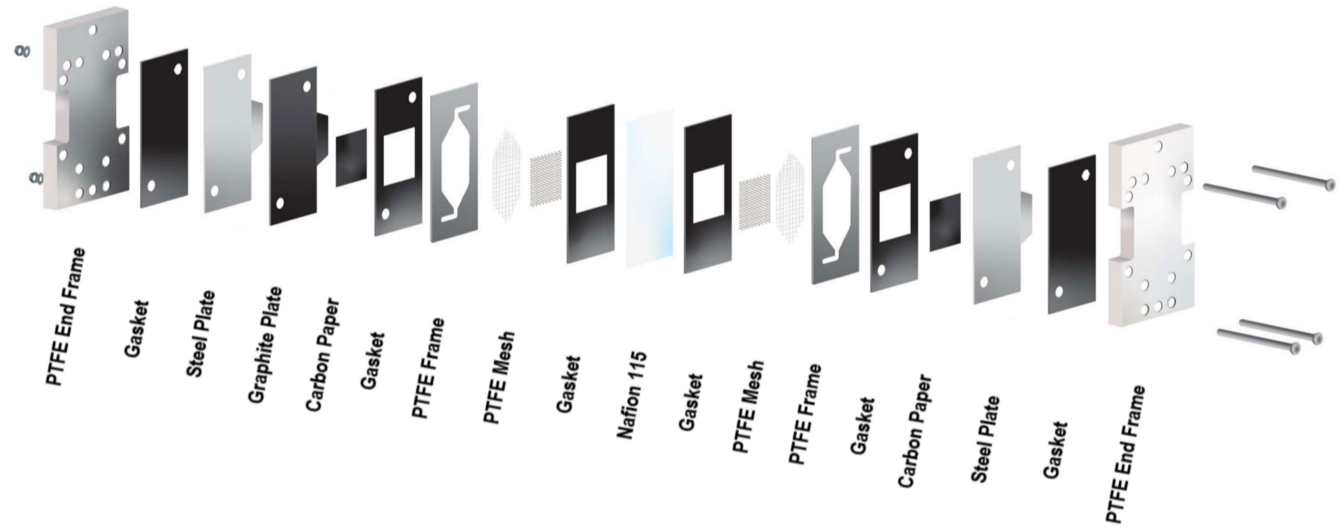

b. Flow Cell Schematic for H_2 Anode-Driven Ni XEC on Gram Scale

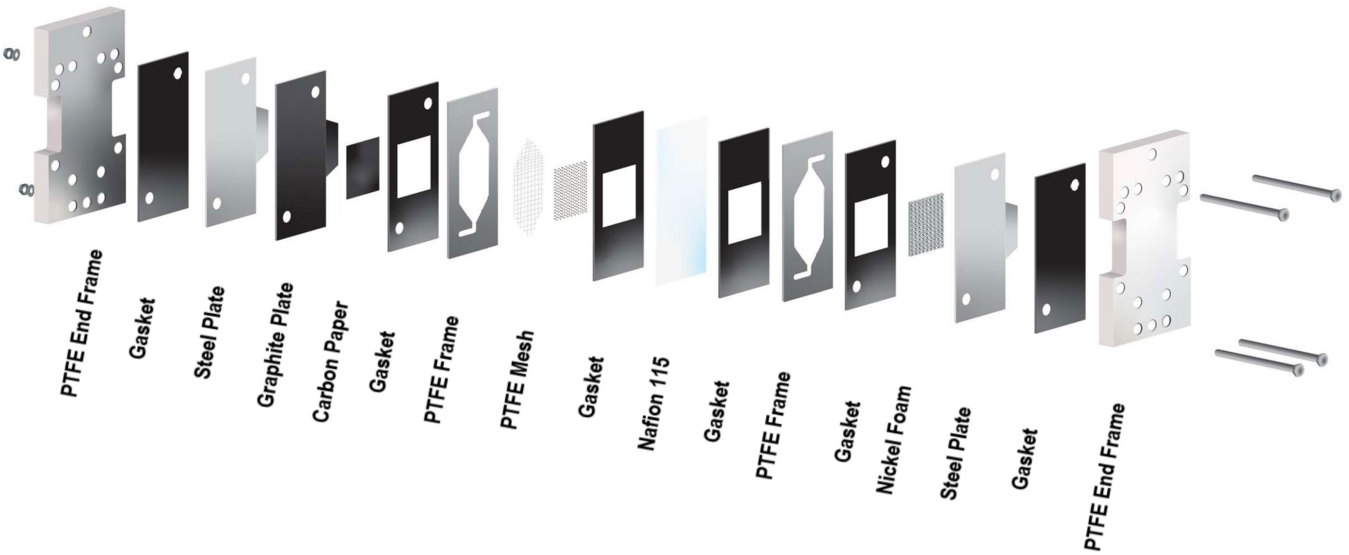

Extended Data Fig. 4 | Schematic representation of electrochemical flow cells used to conduct Ni XEC on the gram scale. a, Schematic depicting the symmetrical flow-cell configuration used for anodic benchmarking with a Bobbitt's salt cathode. Carbon paper and turbulence-promoting mesh are used for both half-cells. **b**, Schematic depicting the flow-cell configuration used for cathodic Ni XEC. A Ni foam cathode was used for the reduction of the Ni catalyst.

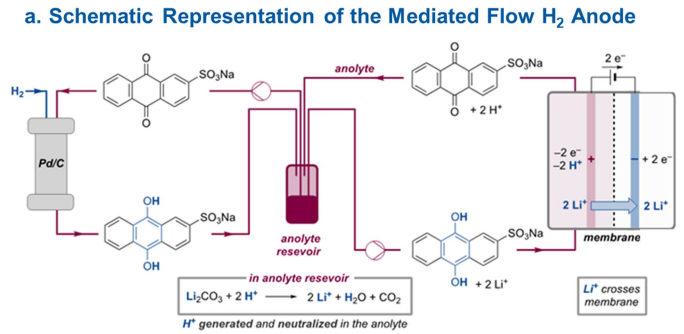

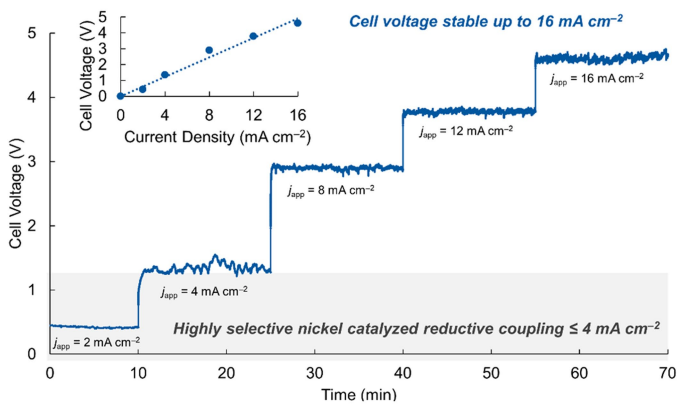

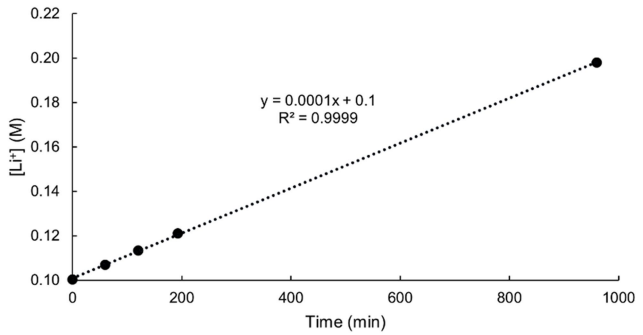

Extended Data Fig. 5 | Schematic representation of the system used to benchmark mediated H_2 anode performance against a Bobbitt's salt cathode with data investigating accessible current densities and ion-transport selectivity. a, Schematic representation of the flow design for gram-scale synthesis using the mediated H_2 anode. One flow loop passes the reservoir solution through a catalytic hydrogenation bed, whereas the other passes the solution through the electrochemical flow cell to enable reduction on the cathode. **b**, Polarization curves benchmarking kinetically accessible rates of electrochemical $AQSH_2$ oxidation. See Fig. 3c for further analysis. **c**, Monitoring of [Li^+] in the cathodic reservoir over time during electrolysis. Aliquots of catholyte solution were analysed using inductively coupled plasma optical emission spectroscopy to determine Li^+ concentration, which is plotted on the *y* axis. See the Supplementary Information for details. We observe the correct starting concentration of 0.1 M, derived from the LiBr electrolyte, followed by a linear increase over time. This is consistent with the selective transport of Li^+ rather than H^+ ions across the Nafion cation-exchange membrane. j_{app}, applied current density.

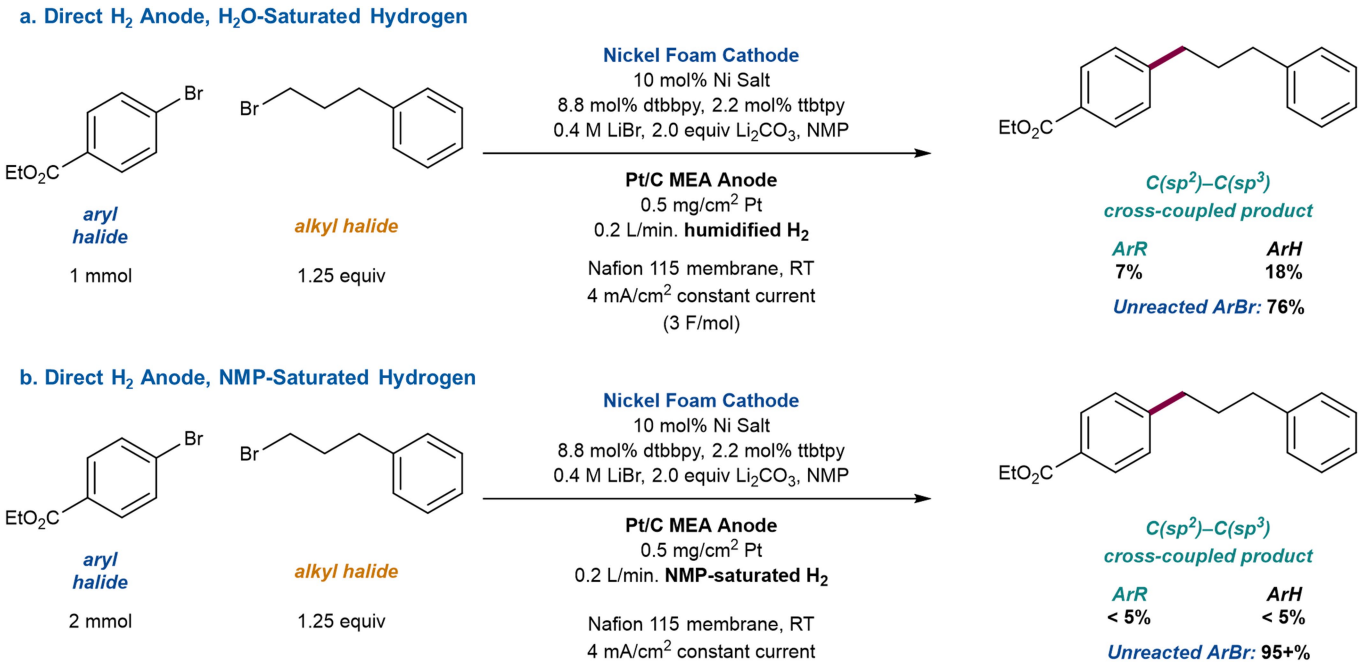

Extended Data Fig. 6 | Ni-catalysed XEC driven by direct application of anodic H_2, conducted using a fuel-cell-inspired cell with an integrated MEA. Gaseous hydrogen was saturated with either H_2O or NMP solvent and used as a terminal reductant without the use of an anodic mediator solution. See the Supplementary Information for detailed methods. **a**, The reaction proceeded with a steady cell voltage of −0.8 V for the allotted time. Both conversion (24%) and product yield (7%), however, were substantially lower than can be achieved using the mediated system (see Extended Data Fig. 3). We speculate that the low faradaic efficiency and the reduced product yield arise from a high rate of proton crossover to the cathode during operation. This flux provides a low-potential reduction reaction in the form of the hydrogen evolution reaction and makes formation of the protodehalogenated side product (18%) the highest-yielding product of Ni-catalysed processes. **b**, To control for any effect from exogenous H_2O, the experiment was repeated with a 'dry' (solvent-saturated) hydrogen source. This approach proved untenable, as the applied cell potential reached the cutoff potential of −8 V within 15 min. This was attributed to rapid desiccation of the Nafion membrane, with solvated protons being transported across the membrane without sufficient replacement of solvent from the anode. RT, room temperature.

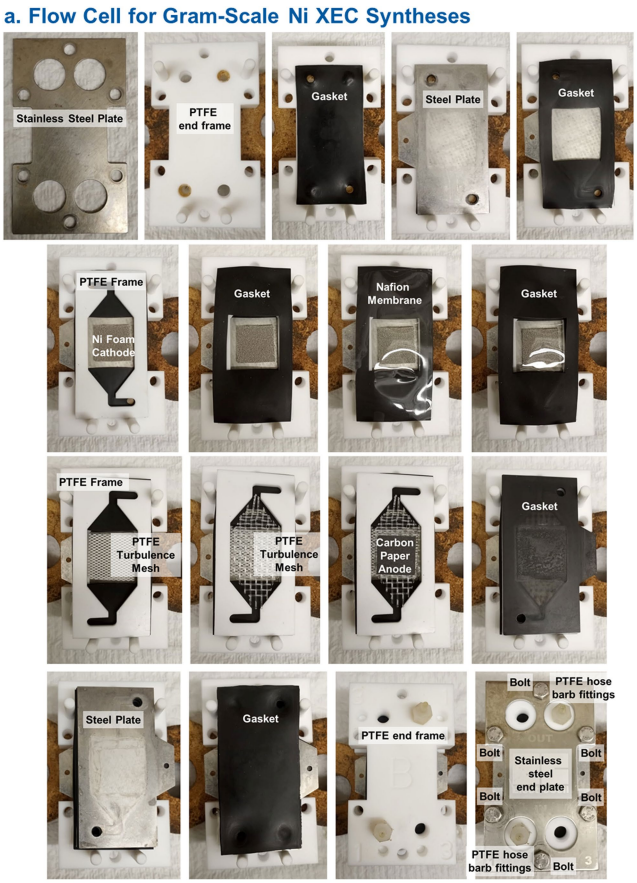

Extended Data Fig. 7 | Electrolysis reactor components used for gram-scale synthesis and reaction time course for Ni XEC. a, Photographs of the assembly of the Electro Syn Cell (from ElectroCell A/S) used for the mediated H_2 system on the gram scale. Viton gaskets are used to separate solid components such as PTFE flow frames, turbulence mesh and 316 SS or graphite electrodes. PTFE and SS end frames are pressed together with bolts to secure the assembly. **b**, Time-course data for a representative Ni-catalysed XEC, depicting the optimized reaction of 1-bromo-3-phenylpropane and ethyl-4-bromobenzoate under optimized conditions: 4 mA cm^{-2}, 0.5 M in Ar–Br substrate.

a. Undivided Screening Apparatus

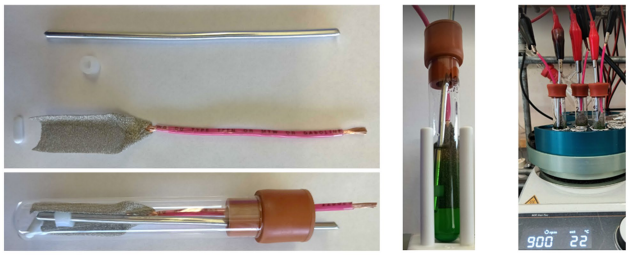

b. Divided H–Cell Screening Apparatus

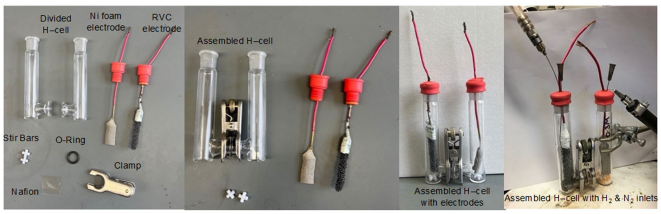

c. Comparison of XEC Reductants in Divided and Undivided Cells

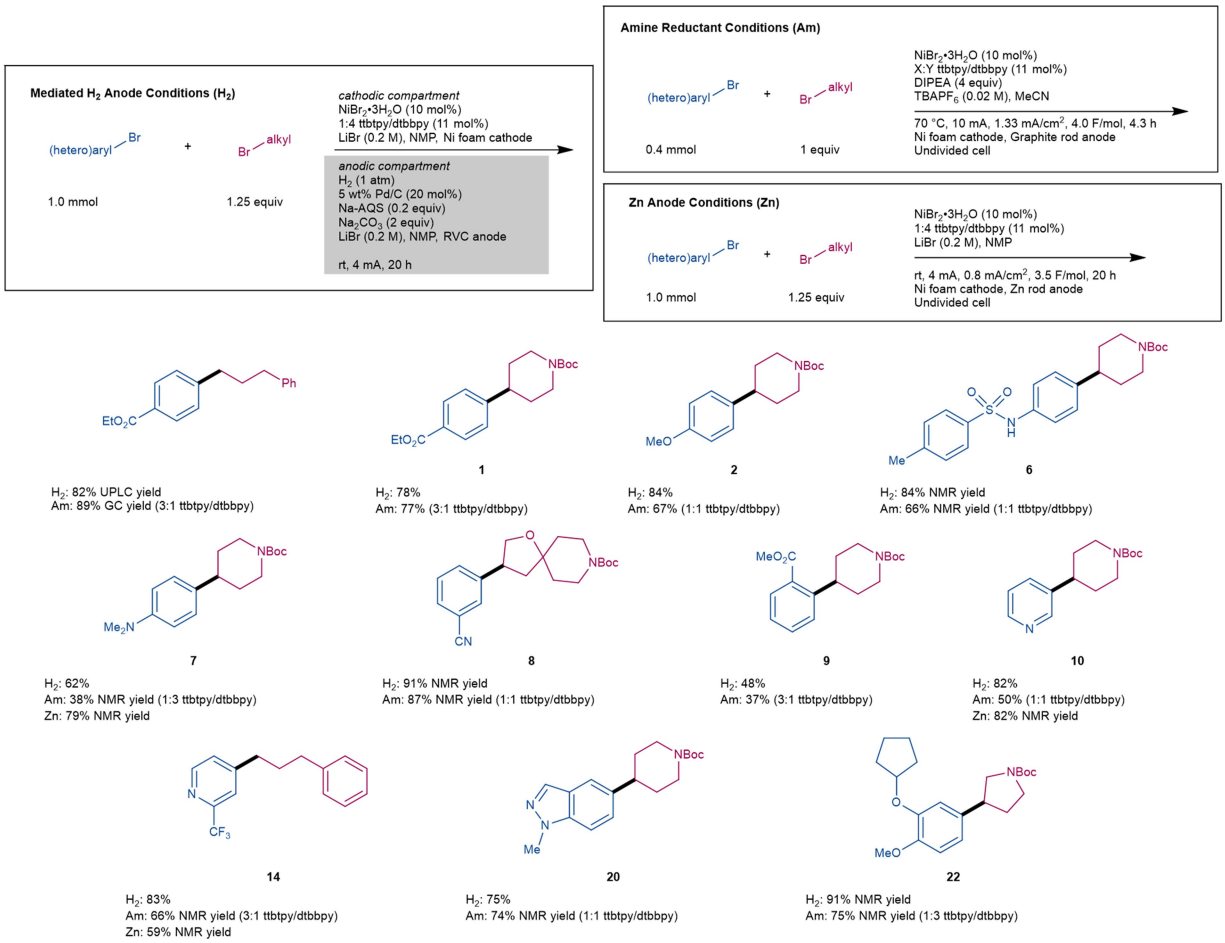

H_2: 82% UPLC yield
Am: 89% GC yield (3:1 ttbtpy/dtbbpy)

1
H_2: 78%
Am: 77% (3:1 ttbtpy/dtbbpy)

2
H_2: 84%
Am: 67% (1:1 ttbtpy/dtbbpy)

6
H_2: 84% NMR yield
Am: 66% NMR yield (1:1 ttbtpy/dtbbpy)

7
H_2: 62%
Am: 38% NMR yield (1:3 ttbtpy/dtbbpy)
Zn: 79% NMR yield

8
H_2: 91% NMR yield
Am: 87% NMR yield (1:1 ttbtpy/dtbbpy)

9
H_2: 48%
Am: 37% (3:1 ttbtpy/dtbbpy)

10
H_2: 82%
Am: 50% (1:1 ttbtpy/dtbbpy)
Zn: 82% NMR yield

14
H_2: 83%
Am: 66% NMR yield (3:1 ttbtpy/dtbbpy)
Zn: 59% NMR yield

20
H_2: 75%
Am: 74% NMR yield (1:1 ttbtpy/dtbbpy)

22
H_2: 91% NMR yield
Am: 75% NMR yield (1:3 ttbtpy/dtbbpy)

Extended Data Fig. 8 | Comparison of reductants for Ni-catalysed XEC. **a**, Two-electrode undivided cells used for screening conventional Zn or amine reductants (Zn anode pictured). See the Supplementary Information for detailed methods. **b**, Two-electrode membrane-divided H-cell for screening of the mediated H_2 anode. **c**, Reaction screening data comparing reductant efficacy. Comparison between amine and mediated H_2 reductants, with the H_2 results disadvantaged by the reporting of isolated rather than assay yields, show that electron-deficient substrates can be coupled in about the same yield with either method but that sterically hindered and electron-rich substrates benefit from the divided mediated H_2 conditions. A subset of these reactions was then further compared with undivided cell reductions with a Zn anode (compare **7**, **10** and **14**). Although some variations were observed, the results reveal comparable or improved efficacy of the mediated H_2 anode relative to other anode systems for electrochemical XEC, as well as providing a foundation for larger-scale applications. DIPEA, Hünig's base; $TBAPF_6$, tetrabutylammonium hexafluorophosphate; rt, room temperature.

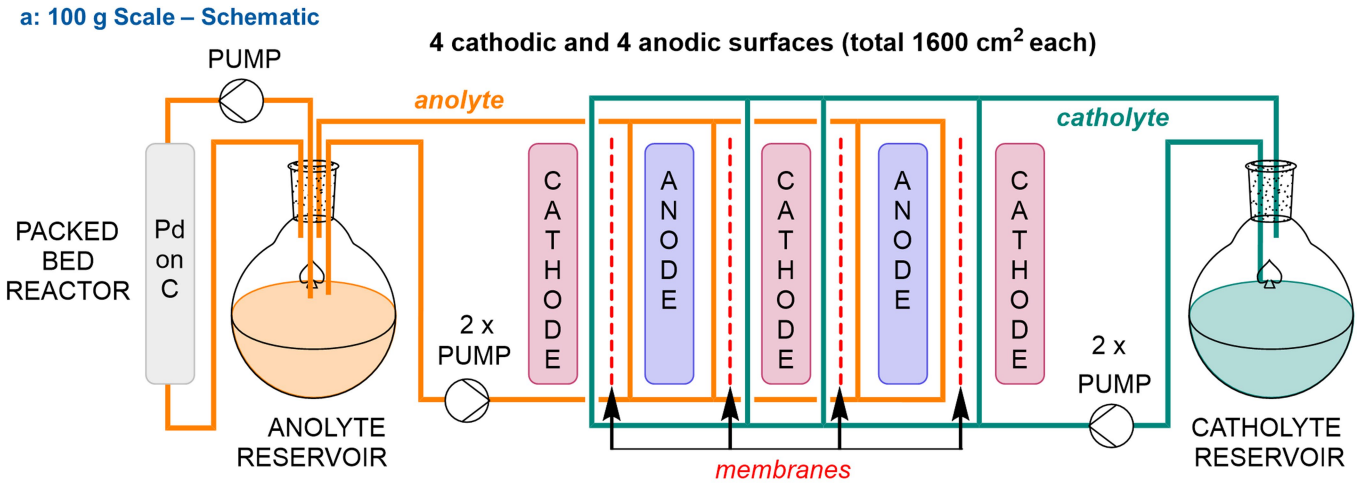

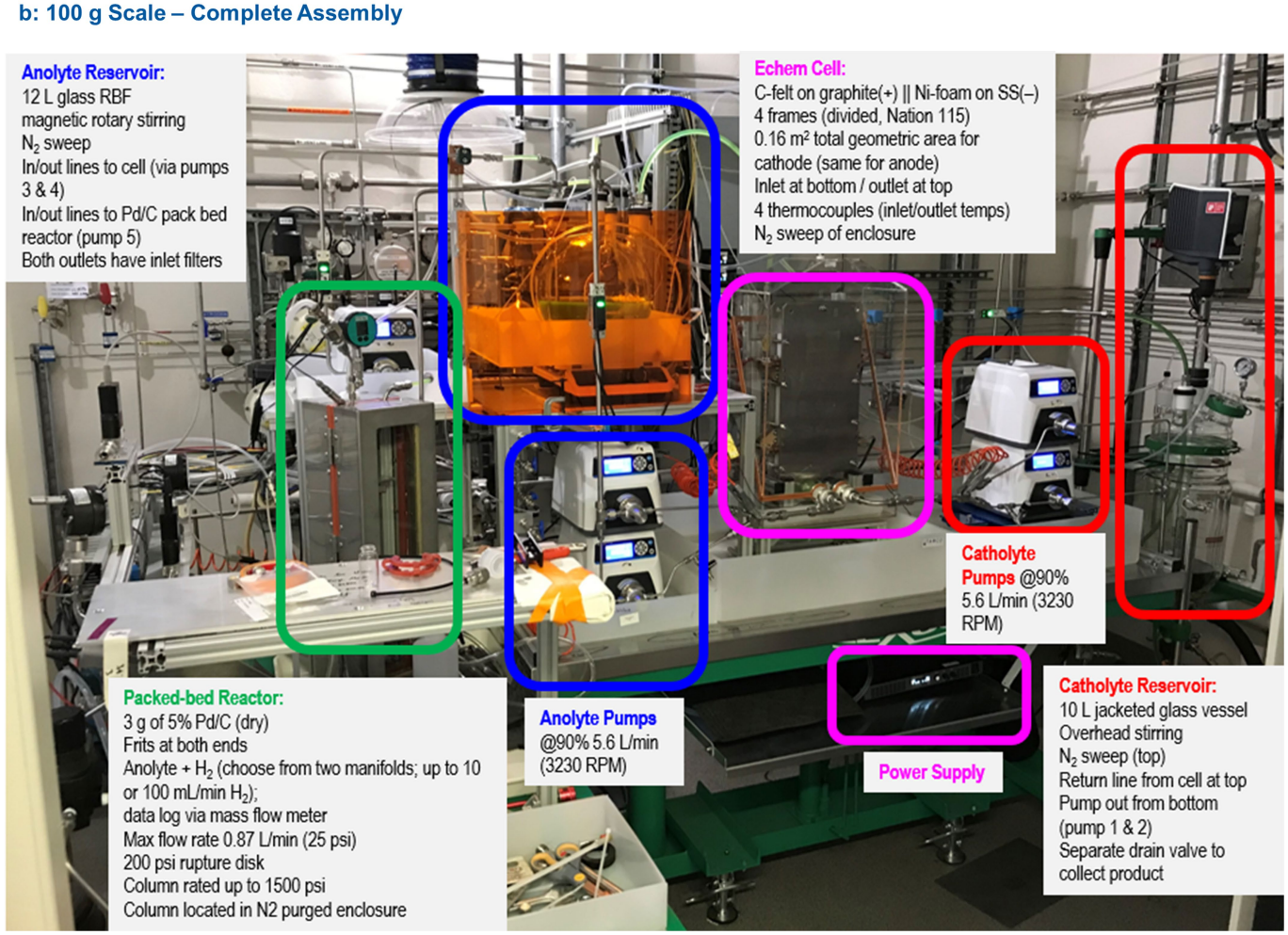

Extended Data Fig. 9 | Reactor system and peripheral components used to conduct Ni XEC on the 100-g scale. a, Schematic depicting the reactor configuration using four sets of parallel electrodes. **b**, Annotated photograph of the fully constituted large-scale flow-reactor system. RBF, round-bottom flask.

a. Flow Cell for 100 g Synthesis of a Cenerimod Intermediate

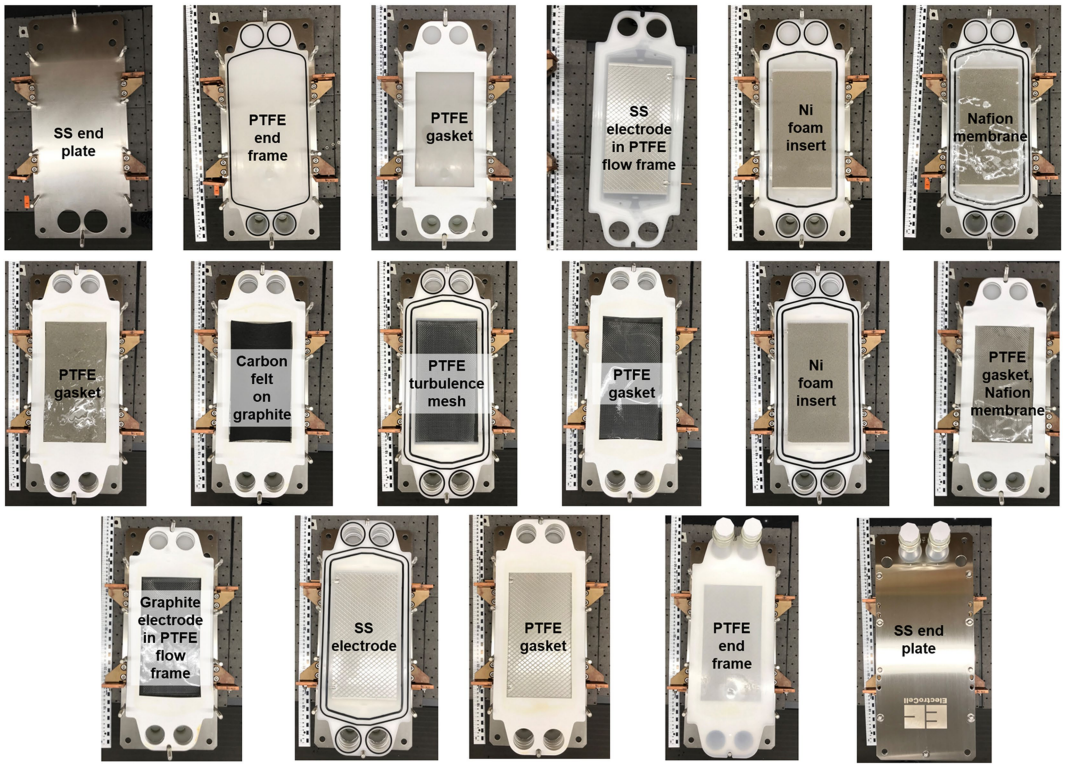

b. Cenerimod Intermediate Synthesis Reaction Tracking

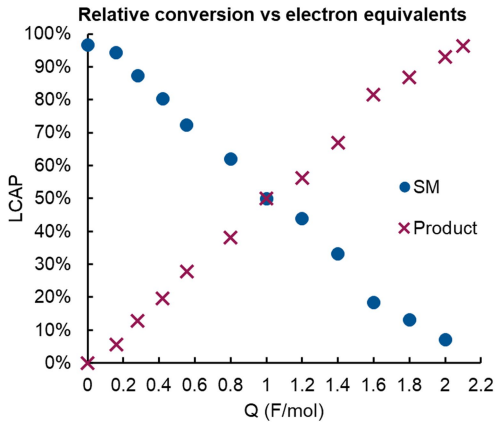

Extended Data Fig. 10 | Electrolysis reactor components used for the synthesis of the cenerimod intermediate on the 100-g scale and associated time-course data. a, Photographs of the assembly of the Electro Syn Cell (from ElectroCell A/S) used for mediated H_2 anode synthesis of the cenerimod intermediate on the 100-g scale. **b**, LCAP data of product and Ar–Cl SM from the 100-g-scale synthesis of the cenerimod intermediate as a function of supplied charge. The reaction was monitored with analysis of cathodic aliquots by UPLC analysis every 20–30 min and the LCAP of the substrate and product were used to roughly monitor the degree of the reaction. LCAP was determined by integrating all SM-related peaks and dividing the area of the product by that combined area. When the reaction reached the cutoff cell voltage of 3 V after just under 4 h, the experiment was stopped. Q, charged passed.